**Journal of Applied Sciences, Information and Computing**

**Volume 4, Issue 1, July 2023**




ISSN: 1813-3509 https://doi.org/10.59568/JASIC-2023-4-1-02

# IMPACTS OF RADIATIVE HEAT FLUX AND HEAT ACQUISITION ON STEADY MAGNETO HYDRODYNAMICS WITH VISCOUS AND OHMIC DISSIPATION, FREE CONVECTION CASSON FLUID FLOW BETWEEN POROUS PLATES

**Usman M.A [1], Lawal O.W [2], Peter, B.A.[3]**

[1] Department of Mathematical Sciences, Olabisi Onabanjo University, Ago-Iwoye, Nigeria
[2] Department of Mathematics, Tai Solarin University of Education, Ijagun, Nigeria
[3] Department of Mathematics and Statistics, Kampala International University, Kampala, Uganda, benjamin.aina@kiu.ac.ug)

## Abstract

An investigation was conducted on a steady magnetohydrodynamic (MHD) free convection flow of a Casson fluid across a parallel vertical plate immersed in a porous medium with viscous and magnetic dissipation. In addition, the energy equation contains terms for radiational heat flow, heat injection, and suction. The perturbation approach provides an analytical solution to the governing nonlinear partial differential equations underlying this phenomenon. The numerical approach in the Maple program was used to verify the correctness of the outcomes produced by the perturbation technique. The Grashof and Prandtl numbers, Casson fluid, magnetic field, and porosity parameters as well as radiation parameter, and heat injection/suction parameter impact on the flow is discussed graphically. Skin friction coefficient and Nusselt number are tabulated for a range of magnetic and radiative parameter values. The other physical factors listed above accelerate the fluid velocity, but the magnetic field decreases it. Furthermore, the wall shear stress and heat transfer were significantly impacted by the magnetic and radiative factors.

**Keywords:** Convection flow with MHD, fluid from Casson, Radiative heat flux, Viscous dissipation, Heat transfer, Ohmic heating, Perturbation technique

## I. INTRODUCTION

This research has caught the interest of many academics because of the numerous uses of the flow of non-Newtonian fluids flow in science and engineering. Although fluids can either be Newtonian or non-Newtonian. The non-Newtonian fluids have wide range of commercial and practical applications, particularly in the processing of materials that contain blood, honey, lubricating oil, and meals. When non-Newtonian fluid is flowing through porous medium, several of these industries are challenged by the magnetic effect.

Recent advances in MHD research have cleared the path for the use and creation of several industries including MHD power generators and the cooling of nuclear reactors which also includes a heat exchanger. The problem of irrigation, heat storage beds, paper industries, petroleum operations, and the production of polymers are a few examples of the uses of MHD of non-Newtonian fluids in porous media.

Casson fluid, which acts like an elastic solid and prevents flow in the presence of modest shear stresses, is obviously one of the instances of non-Newtonian fluids. In order to determine the flow behavior of suspended pigment oil, Casson developed the Casson fluid model in 1959. The magnitude of the Casson fluid's shear stress must be greater than the yield shear stress in order to determine the fluid's flow. The two-phase suspension used in the Casson model demonstrates how the solid and liquid phases interact in a beneficial way.

Example of Casson fluids is tomato paste, red blood cells, fibrinogen, proteins, and globulin among others. Chemicals used in the manufacture of pharmaceuticals, paints, coal, synthetic lubricants, and China clay all employ Casson fluid. Makanda et al. (2015) recently looked at how radiation affected MHD free convection flow from a cylinder with partial slip. It was shown that the existence of the velocity slip factor was amplified by the decline in velocity profile brought on by the increases in magnetic field.

Talha et al. (2021) considered an unstable MHD flow model. They looked at the fluid condition at ramped temperature and velocity, and they presented a visual comparison of the solutions for ramped and constant conditions at the wall. Khalid et al. (2015), explored a Casson fluid flow across vertical plate that was oscillating while maintaining a constant temperature without the use of MHD. The outcomes met the necessary criteria for non-Newtonian fluid and reduced the Newtonian fluid solution to a special case, satisfying the relevant conditions for that fluid type. With consideration of viscous dissipation in two dimensions, Hammad et al. (2020), used a nonlinear stretching surface to show the impact of heat absorption or suction on the MHD boundary layer flow of Casson Nanofluid. Hymavaths and Sridhar (2016) used the Keller box approach to examine the effects of MHD Casson fluid flow over a porous stretched sheet in the presence of chemical processes. They observed that when the suction parameter rose, the concentration profile rapidly fell in comparison to the fluid's velocity. In a rotating permeable microchannel with wall slip and hall current, Eegunjobi and Makinde (2020) looked at the intrinsic irreversibility of Casson fluid flow. They discovered that the rate of entropy creation is enhanced by fluid rotation and velocity slip but decreases with an increase in magnetic field strength. Rao and Sreenadh (2017), looked at the flow of Casson fluid in constant two-dimensional MHD-free convective boundary layer over a permeable stretched surface. Thermal radiation as well


https://doi.org/10.59568/JASIC-2023-4-1-02

as chemical reactions, assuming that temperature, wall concentration, and stretching velocity would all change according to a particular exponential form.

In the present work, we investigate the steady Casson fluid flow of MHD over a parallel vertical plate positioned in a porous medium with viscous and magnetic dissipation. The nonlinear differential equation that resulted from the study was converted into an ordinary differential equation by utilizing the regular perturbation approach, and it was then analytically solved.

Heat transfer study provided an example of the value of radiation flux and heat injection or suction. The skin friction, Nusselt number and other thermophysical parameters were provided. The result of non-linear equations was solved analytically and the effects of various thermophysical parameters were shown graphically.

The constant MHD-free convective flow of Casson fluid over a parallel vertical plate set in porous media with viscous and magnetic dissipation along with radiation effects were investigated. We chose a certain coordinate with the electrically non-conducting plates' -axis running parallel to them and the -axis perpendicular to them. Since the flow's Reynolds number is so low, the impact of the induced magnetic field is disregarded. This is accurate because partly ionized gases have a very low magnetic Reynolds number. In compared to the radiative heat flow normal to the plate, the radiative heat flux along with direction of the plate was disregarded. Since there was no consideration of an electric field, the fluid's polarization impact was also disregarded. Below is the Cauchy stress tensor

$$\tau_{xy} = \begin{cases} 2\left(\mu_\beta + \frac{p_y}{\sqrt{2\pi}}\right)e_{xy} & \pi > \pi_c \\ 2\left(\mu_\beta + \frac{p_y}{\sqrt{2\pi_c}}\right)e_{xy} & \pi < \pi_c \end{cases} \quad (1)$$

where $\pi = e_{xy}$ is the $(x, y)^{xh}$ component of the deformation rate, $\pi$ and $\pi_c$ are the deformation rate and non-Newtonian [parameter respectively, $p_y$ is yield stress of the fluid and $\mu_\beta$ is the plastic dynamic viscosity of non-Newtonian fluid. When deriving the governing equation, we assume that;

(i) the two plates are stationary, (ii) the flow is steady incompressible unidirectional and one dimensional, (iii) the fluid is non-Newtonian and free convective with viscous and magnetic dissipation taken into consideration in energy equation. These assumptions resulted to the following set of nonlinear differential equation

$$\frac{\partial v}{\partial y} = 0 \text{ i.e. } v = -v_0 \text{(constant)} \quad (2)$$

$$\frac{\partial p}{\partial y} = 0 \Rightarrow p \text{ is independent of } y$$


https://doi.org/10.59568/JASIC-2023-4-1-02

$$\rho v\frac{\partial u}{\partial y}=\mu_\beta\left(1+\frac{1}{\alpha}\right)\frac{\partial^2 u}{\partial y^2}-\sigma B_0^2 u-\mu_\beta\frac{\left(1+\frac{1}{\alpha}\right)\phi}{k}u+\rho g\beta_T\left(T-T_\infty\right) \tag{3}$$

$$\rho c_p v\frac{\partial T}{\partial y}=k_1\frac{\partial^2 T}{\partial y^2}+\mu_\beta\left(1+\frac{1}{\alpha}\right)\left(\frac{\partial u}{\partial y}\right)^2+\sigma B_0^2 u^2-\frac{\partial q_r}{\partial y}-Q_0\left(T-T_\infty\right) \tag{4}$$

with the following boundary conditions

$$u=0,\qquad T=T_w \text{ at } y=0 \tag{5}$$

$$u\to 0,\qquad T\to T_\infty \text{ as } y\to\infty$$

where $u$ and $v$ are velocities in x and y directions, $T$ -temperature, $\alpha=\mu_\beta\sqrt{2\pi_c}/p_y$ is the Casson parameter, $\rho$ -fluid density, $g$ is the acceleration due to gravity, $\beta_T$ represent the coefficient of thermal expansion, $\sigma$ -the fluidelectrical conductivity, $k$ and $\phi$ are permeability and porosity of the fluid respectively, $B_0$ is the magnetic flux density, $c_p$ is the specific heat capacity, $T_\infty$ is the free stream temperature, $T_w$ is the wall temperature, $q_r$ - heat flux, $Q_0$-heat absorption coefficient and subscripts $w$ and $\alpha$ are called surface and ambient condition respectively.

The radiactive heat flux is obtained from Rosseland approximation as

$$q_r=-\frac{4\sigma_1}{3k_2}\frac{\partial T^4}{\partial y} \tag{6}$$

where $\sigma_1$ represent Stefan-Bultzman constant and $k_2$ is the absorption coefficient. Using (6) simply mean that we consider optically thick fluid in our analysis.

$$T^4\approx 4T_\infty^3 T-3T_\infty^4 \tag{7}$$

Equation (6) is widely apply in computational fluid dynamics (CFD) when it involves radiation absorption problem in formulation of term $T^4$ as a linear function.

Substituting (6) and (7) in (4), we obtain

$$\rho c_p v\frac{\partial T}{\partial y}=\left(k_1+\frac{16\sigma_1 T_\infty^3}{3k_2}\right)\frac{\partial^2 T}{\partial y^2}+\mu_\beta\left(1+\frac{1}{\alpha}\right)\left(\frac{\partial u}{\partial y}\right)^2+\sigma B_0^2 u^2-Q_0\left(T-T_\infty\right) \tag{8}$$


https://doi.org/10.59568/JASIC-2023-4-1-02

Introducing the non-dimensional variables

$$y = \frac{v_0 \bar{y}}{\upsilon}, \qquad u = \frac{\bar{u}}{v_0}, \theta = \frac{T - T_\infty}{T_w - T_\infty}, \tag{9}$$

Substituting (9) into (3) and (8) and dropping "-", we obtained the following non-dimensional equations

$$\left(1 + \frac{1}{\alpha}\right)\frac{\partial^2 u}{\partial y^2} + \frac{\partial u}{\partial y} - \left[M + \frac{\left(1 + \frac{1}{\alpha}\right)}{K}\right]u + Gr\,\theta = 0 \tag{10}$$

$$(1 + Ra)\frac{\partial^2 \theta}{\partial y^2} + \Pr\frac{\partial \theta}{\partial y} + Ec\left[\left(1 + \frac{1}{\alpha}\right)\left(\frac{\partial u}{\partial y}\right)^2 + Mu^2\right] + \Pr Q_1 \theta = 0 \tag{11}$$

where;

$$M = \frac{\sigma B_0^2 \upsilon^2}{v_0^2 \mu}, \quad K = \frac{k_1 v_0^2}{\phi \upsilon^2}, \qquad Gr = \frac{\rho g \beta_T (T_w - T_\infty)}{v_0^2 \mu}, \quad Ra = \frac{16\sigma_1 T_\infty^3}{3k_2 k_1},$$

$$\Pr = \frac{\mu c_p}{k_1}, \; Q_1 = \frac{Q_0 \upsilon}{\rho c_p v_0^2} \; Ec = \frac{v_0^2}{c_p (T_w - T_\infty)}.$$

The corresponding boundary conditions in dimensionless form are

$$u = 0, \qquad \theta = 1 \text{ at } y = 0 \tag{12}$$

$$u \to 0, \qquad \theta \to 0 \text{ as } y \to \infty$$

## II METHOD OF SOLUTION

In an incompressible fluid flow, $0 < Ec < 1$ since the flow due to the Joule dissipation is super imposed on the main flow.

We apply the perturbation technique by assuming the following


https://doi.org/10.59568/JASIC-2023-4-1-02

$$u(y) = u_0(y) + Ecu_1(y) + O(Ec^2)$$
$$\theta(y) = \theta_0(y) + Ec\theta_1(y) + O(Ec^2) \tag{13}$$

Putting (13) into equations (10) – (12) and equating the coefficient of zeroth and first order base on the power of $Ec$ and neglecting the term $+O(Ec^2)$, we have the following ODE:

$$\left(1+\frac{1}{\alpha}\right)\frac{\partial^2 u_0}{\partial y^2} + \frac{\partial u_0}{\partial y} - \left[M + \frac{\left(1+\frac{1}{\alpha}\right)}{K}\right]u_0 + Gr\theta_0 = 0 \tag{14}$$

with the boundary condition

$$y = 0: u_0 = 0, \quad y \to 1: u_0 = 0 \tag{15}$$

$$(1+Ra)\frac{\partial^2 \theta_0}{\partial y^2} + \Pr\frac{\partial \theta_0}{\partial y} + \Pr Q_1\theta_0 = 0 \tag{16}$$

with the boundary condition

$$y = 0: \theta_0 = 1, \quad y \to 1: \theta_0 = 0 \tag{17}$$

$$\left(1+\frac{1}{\alpha}\right)\frac{\partial^2 u_1}{\partial y^2} + \frac{\partial u_1}{\partial y} - \left[M + \frac{\left(1+\frac{1}{\alpha}\right)}{K}\right]u_1 + Gr\theta_1 = 0 \tag{18}$$

with the boundary condition

$$y = 0: u_1 = 0, \quad y \to 1: u_1 = 0 \tag{19}$$

$$(1+Ra)\frac{\partial^2 \theta_1}{\partial y^2} + \Pr\frac{\partial \theta_1}{\partial y} + \left[\left(1+\frac{1}{\alpha}\right)\left(\frac{\partial u_0}{\partial y}\right)^2 + Mu_0^2\right] + \Pr Q_1\theta_1 = 0 \tag{20}$$

with the boundary condition

$$y = 0: \theta_1 = 0, \quad y \to 1: \theta_1 = 0 \tag{21}$$


https://doi.org/10.59568/JASIC-2023-4-1-02

The solution of (14), (16), (18) and (20) with boundary condition (15), (17), (19) and (21) respectively are

$$u_0 = \sum_{n=0}^{\infty}\left[\frac{1}{n!}\left(a_8 a_1^n + a_9 a_9^n + c_3 a_4^n + c_4 a_4^n\right)\right]y^n \tag{22}$$

$$\theta_0 = \sum_{n=0}^{\infty}\left[\frac{1}{n!}\left(c_1 a_1^n + c_2 a_2^n\right)\right]y^n \tag{23}$$

Furthermore, when $n = 1, 2, \ldots\ldots 5$, we obtained

$$\begin{aligned}\theta_1 &= c_6 \sin(a_{15}y) + c_5 \cos(a_{15}y) + a_{24}y^8 + a_{23}y^7 + a_{22}y^6 + a_{21}y^5 + a_{20}y^4 + a_{19}y^3 \\ &\quad + a_{18}y^2 + a_{17}y + a_{16}\end{aligned} \tag{24}$$

$$\begin{aligned}u_1 &= \left(a_{53}e^{a_{54}y} + a_{52}e^{a_{55}y}\right)y^8 + \left(a_{51}e^{a_{55}y} + a_{50}e^{a_{54}y}\right)y^7 + \left(a_{49}e^{a_{55}y} + a_{48}e^{a_{54}y}\right)y^6 \\ &\quad + \left(a_{47}e^{a_{55}y} + a_{46}e^{a_{54}y}\right)y^5 + \left(a_{45}e^{a_{54}y} + a_{44}e^{a_{55}y}\right)y^4 + \left(a_{43}e^{a_{54}y} + a_{42}e^{a_{55}y}\right)y^3 \\ &\quad + \left(a_{41}e^{a_{55}y} + a_{40}e^{a_{54}y}\right)y^2 + \left(a_{39}e^{a_{55}y} + a_{38}e^{a_{54}y}\right)y + \left[\begin{matrix}(\sin(a_{15}y)a_{37} + a_{33}\cos(a_{15}y)) \\ + a_{32}\end{matrix}\right]e^{a_{55}y} \\ &\quad + c_8 e^{a_{25}y} + a_{34}e^{a_{54}y} + c_7 e^{a_{26}y} + a_{35}\cos(a_{15}y)e^{a_{54}y} + a_{36}\sin(a_{15}y)e^{a_{54}y}\end{aligned} \tag{25}$$

Hence

$$u(y) = \sum_{n=0}^{\infty}\left[\frac{1}{n!}\left(a_8 a_1^n + a_9 a_9^n + c_3 a_4^n + c_4 a_4^n\right)\right]y^n + Ec\begin{bmatrix}\left(a_{53}e^{a_{54}y} + a_{52}e^{a_{55}y}\right)y^8 + \left(a_{51}e^{a_{55}y} + a_{50}e^{a_{54}y}\right)y^7 \\ + \left(a_{49}e^{a_{55}y} + a_{48}e^{a_{54}y}\right)y^6 + \left(a_{47}e^{a_{55}y} + a_{46}e^{a_{54}y}\right)y^5 \\ + \left(a_{45}e^{a_{54}y} + a_{44}e^{a_{55}y}\right)y^4 + \left(a_{43}e^{a_{54}y} + a_{42}e^{a_{55}y}\right)y^3 \\ + \left(a_{41}e^{a_{55}y} + a_{40}e^{a_{54}y}\right)y^2 + \left(a_{39}e^{a_{55}y} + a_{38}e^{a_{54}y}\right)y \\ + \left[\begin{matrix}(\sin(a_{15}y)a_{37} + a_{33}\cos(a_{15}y)) \\ + a_{32}\end{matrix}\right]e^{a_{55}y} + c_8 e^{a_{25}y} \\ + a_{34}e^{a_{54}y} + c_7 e^{a_{26}y} + a_{35}\cos(a_{15}y)e^{a_{54}y} + a_{36} \\ \sin(a_{15}y)e^{a_{54}y}\end{bmatrix} \tag{26}$$


https://doi.org/10.59568/JASIC-2023-4-1-02

$$\theta(y)=\sum_{n=0}^{\infty}\left[\frac{1}{n!}\left(c_1a_1^n+c_2a_2^n\right)\right]y^n+Ec\begin{bmatrix}c_6\sin(a_{15}y)+c_5\cos(a_{15}y)+a_{24}y^8\\+a_{23}y^7+a_{22}y^6+a_{21}y^5+a_{20}y^4+a_{19}y^3\\+a_{18}y^2+a_{17}y+a_{16}\end{bmatrix} \quad (27)$$

The skin friction factor $(\tau)$ at the plate $y=0$ is given as

$$\begin{aligned}\tau&=\left.\frac{\partial u}{\partial y}\right|_{y=0}\\&=a_{35}a_{54}+a_{15}a_{36}+a_{15}a_{37}+c_8a_{25}+c_7a_{26}+(a_{33}+a_{32})a_{55}+a_3c_3+a_4c_4\\&+a_{34}a_{54}+a_9a_2+a_8a_1+a_{38}+a_{39}\end{aligned} \quad (28)$$

The Nusselt number $(Nu)$ which is the rate of heat transfer based on Fourier's law of heat conduction is given as

$$\begin{aligned}Nu&=-\left.\frac{\partial\theta}{\partial y}\right|_{y=0}\\&=c_1a_1+c_2a_2+c_6a_{15}+a_{17}\end{aligned}$$

## III RESULTS AND DISCUSSION

When heat is transferred from the two plates into the boundary layer by free convection current, the numerical evaluation and approximate analytical results of the problem were discussed and presented graphically in Figures 1–8. Figure 1 narrate different values of $\alpha$ for velocity profile. The fluid increases due to the plasticity of Casson fluid. In Figure 2, increase in the value of $Gr$ due to enhancement in the buoyance for

Figure 3 depicted that velocity profile increases with increase in radiation parameter $Ra$. This is because increase in velocity at the boundary layer decreases the boundary layer thickness. Figure 4 revealed that increase in magnetic parameter $M$ reduces the velocity profile due to the presence of Lorentz force that decelerate the flow.

Figure 5 depicts that increase in the value of $K$ have a considerable effect on the fluid permeability which consequently reduced the porous medium which allow the flow velocity to be increased, thereby heighten the velocity field.

It was shown in Figure 6 that as $\Pr$ increases, the temperature profile decreases. This is because thermal conductivity of the fluid reduces with increase in $\Pr$ thereby reduces the thermal boundary layer thickness. The temperature profile for various value of $Ra$ was presented in Figure 7. It was revealed that increase in $Ra$ results to decrease in the boundary layer thickness which reduces the value of heat transfer in the presence of thermal forces. Similarly, in Figure 8, the effects of increasing in $Q_1$ results to increase


https://doi.org/10.59568/JASIC-2023-4-1-02

in temperature profile due to rises in the amount of heat injection.

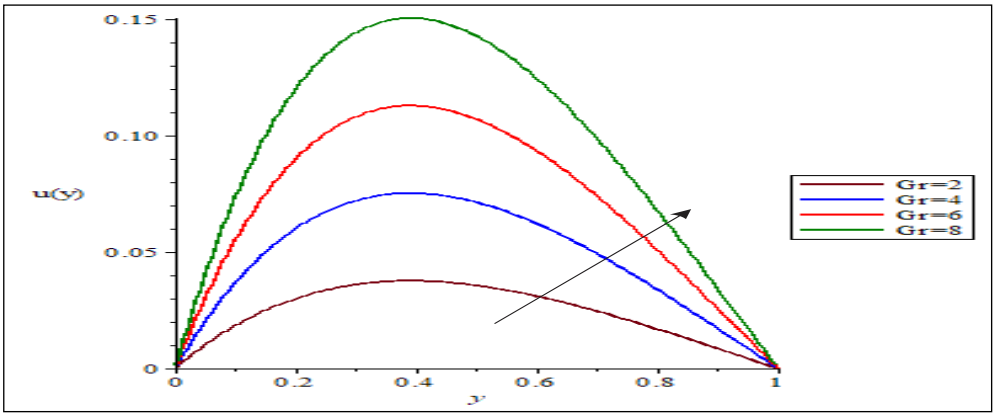


**Figure 1.** Graph of the velocity profile for various value $\alpha$ when $\Pr = 0.71,\ K = 0.5,\ M = 2.0\ Gr = 2.0,\ Q_1 = 2.0$ and $Ra = 0.5$

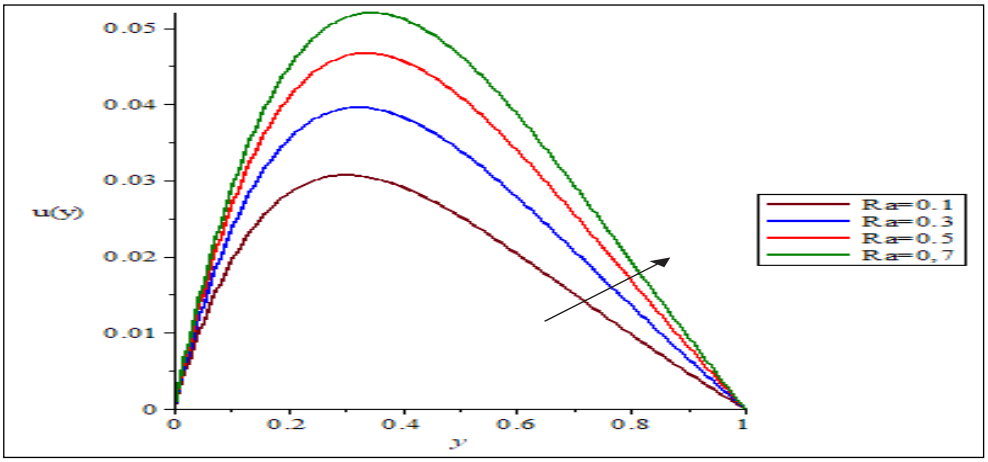


**Figure 2.** Graph of the velocity profile for various value $Gr$ when $\Pr = 0.71,\ K = 0.5,\ M = 2.0\ \alpha = 0.6,\ Q_1 = 2.0$ and $Ra = 0.5$


https://doi.org/10.59568/JASIC-2023-4-1-02

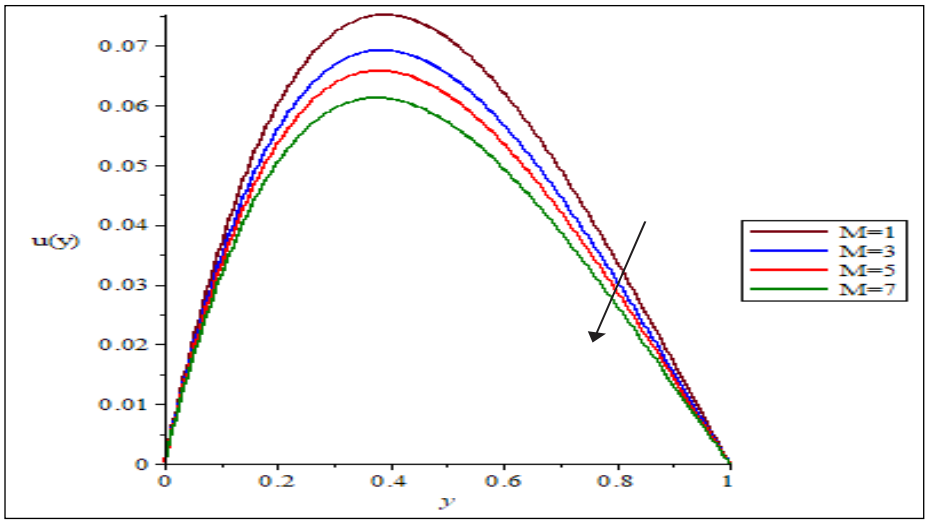


**Figure 3.** Graph of the velocity profile for various value $Ra$ when $\Pr = 0.71,\ K = 0.5,\ M = 2.0,\ \alpha = 0.6,\ Q_1 = 2.0$ and $Gr = 2.0$

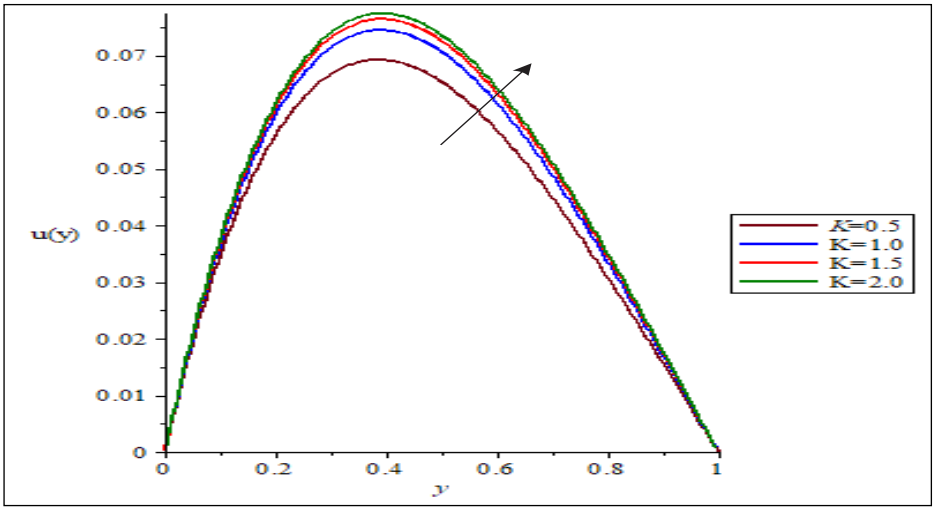


**Figure 4.** Graph of the velocity profile for various value $M$ when $\Pr = 0.71,\ K = 0.5,\ Gr = 2.0,\ \alpha = 0.6,\ Q_1 = 2.0$ and $Ra = 0.5$


https://doi.org/10.59568/JASIC-2023-4-1-02

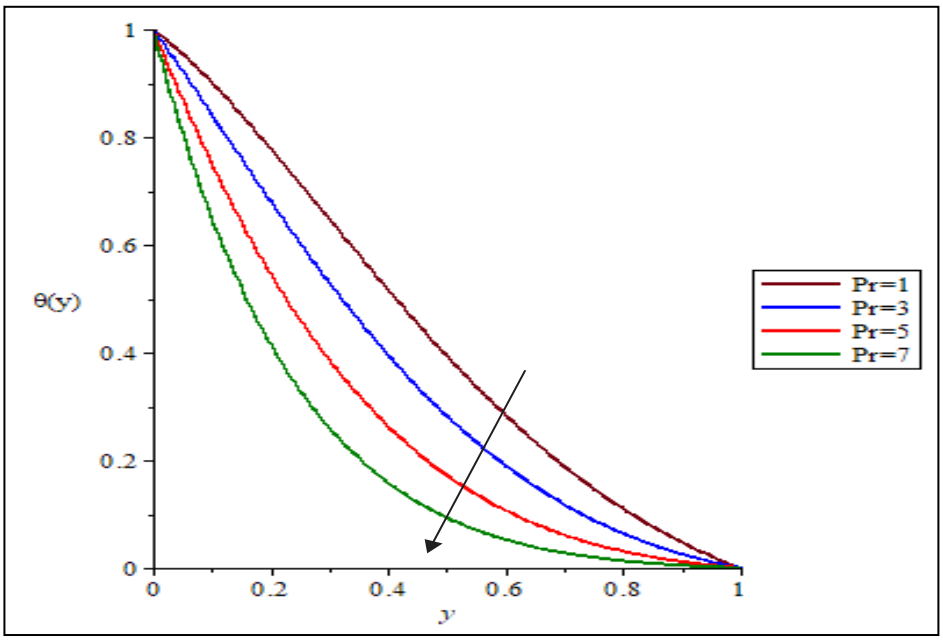


**Figure 5.** Graph of the temperature profile for various value Pr when $K = 0.5,\ M = 2.0,\ Gr = 2.0\quad \alpha = 0.6,\ Q_1 = 2.0$ and $Ra = 0.5$

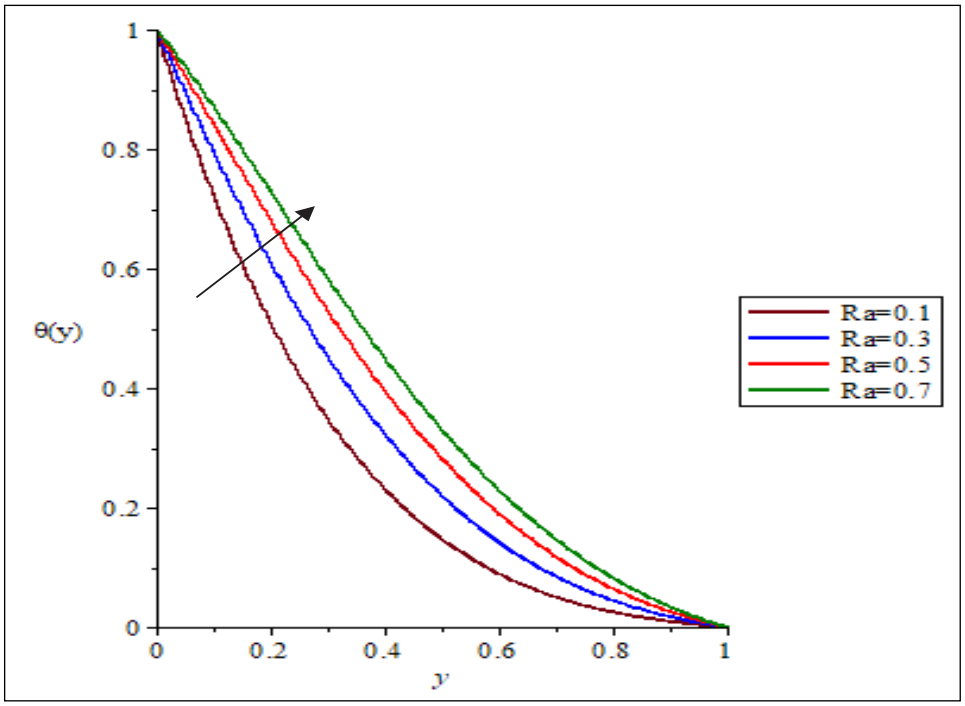


**Figure 6.** Graph of the temperature profile for various value $Ra$ when $K = 0.5,\ M = 2.0,\ Gr = 2.0, \alpha = 0.6,\ Q_1 = 2.0$ and $\Pr = 0.71$


https://doi.org/10.59568/JASIC-2023-4-1-02

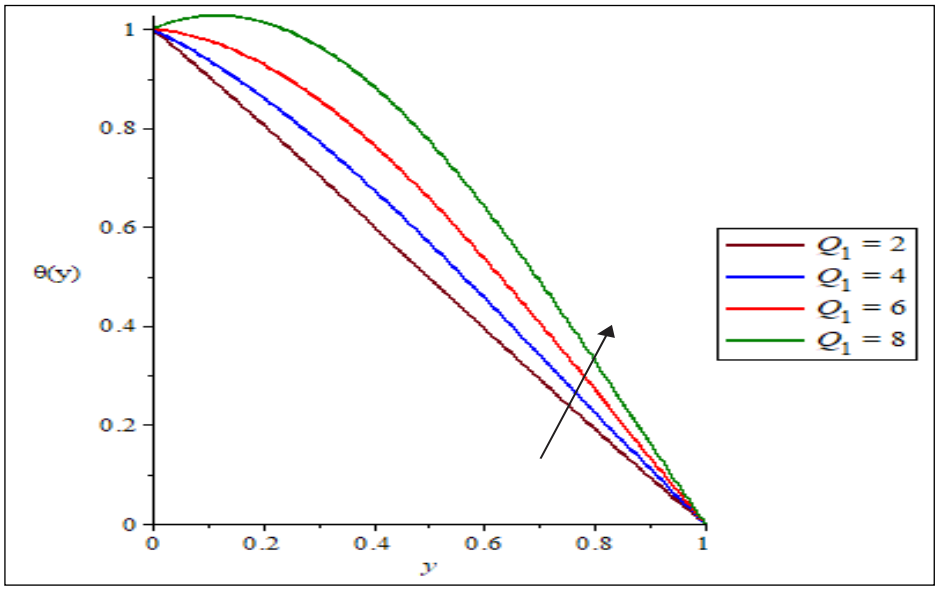


**Figure 7.** Graph of the temperature profile for various value $Q_1$ when $K = 0.5,\ M = 2.0,\ Gr = 2.0,\ \alpha = 0.6,\ Ra = 0.5$ and $\Pr = 0.71$

**Table 1**. Validation of analytical solution and numerical solution for local skin friction and heat transfer coefficient

| $M$ | Approximate Analytical Results | | Numerical Results | |
|---|---|---|---|---|
| | $\tau$ | $Nu$ | $\tau$ | $Nu$ |
| 1.0 | 0.2277901098 | 0.9204995619 | 0.2277899744 | 0.9205005660 |
| 3.0 | 0.2193514642 | 0.9204992673 | 0.2193512694 | 0.9205010179 |
| 5.0 | 0.2117623583 | 0.9204987894 | 0.2117620996 | 0.9205014341 |
| 7.0 | 0.2048939203 | 0.9204980901 | 0.2048935965 | 0.9205018185 |


https://doi.org/10.59568/JASIC-2023-4-1-02

**Table 2**. Validation of analytical solution and numerical solution

| $Ra$ | Approximate Analytical Results | | Numerical Results | |
|---|---|---|---|---|
| | $\tau$ | $Nu$ | $\tau$ | $Nu$ |
| 0.1 | 0.2050516901 | 0.8918113362 | 0.2050512659 | 0.8918160181 |
| 0.3 | 0.2049687794 | 0.9083140372 | 0.2049684057 | 0.9083182049 |
| 0.5 | 0.2048939202 | 0.9204980910 | 0.2048935965 | 0.9205018185 |
| 0.7 | 0.2048291813 | 0.9298472462 | 0.2048288876 | 0.9298505984 |

Finally, table 1 and 2 confirmed the validity and accuracy of the results obtained in this study and compared it with those obtained using Maple software for local skin – friction coefficient ($\tau$) and Nusselt number ($Nu$). These tables also reveal that there is a strong correlation between the two outcomes, demonstrating the validity of the study's methodology. In Table 1, it is shown that and slightly decrease as increases, but in Table 2, a rise in both lowers and raises the values of and, respectively.

## IV CONCLUSION

The findings of the measured velocity and temperature profiles are examined and illustrated. The following are the final conclusions:

1. Velocity of the fluid increases with increase in Casson fluid parameter ($\alpha$) and Grasshof number ($Gr$).
2. Porosity parameter ($K$) and magnetic parameter ($M$) have a great influence in the increment and decrement of fluid velocity respectively.
3. The temperature of the fluid reduces when the Prandtl number ($\Pr$) and heat injection/suction parameter ($Q_1$) increases.
4. The skin – friction ($\tau$) is slightly decreased with increase in magnetic parameter ($M$) and radiation parameter ($Ra$)
5. Heat transfer rate ($Nu$) rises as magnetic parameter ($M$) and radiation parameter ($Ra$) increases.

## V REFERENCES

[1] Casson N. (1959), “A flow of equation for pigment suspension of (ed Mill, C,C)” 84-104. Pergamon Press, Oxford.

[2] Makanda, G., Shaw, S. &Sibanda P. (2015). “Effects of radiation on MHD free convection”,Doi:186/s13661-015-0333-5

[3] Talha, A., Kuman, P. &Watthayu W. (2021). Unsteady MHD Scientific Reports. Doi:101038/s41598-021-83691-2

[4] Khalid, A., Khan, I., Khan, A. &Shafie S. (2015). Unsteady MHD free convection flow. Engineering Science and Technology, an International Journal. **30**(1), 1-9.

[5] Afikuzzaman, M. &Alam N. (2016). MHD Casson fluid flow International Journal of Science and Technology. **21**(1), 59-10.

[6] Hammad, A., Saheed, A., Mohamed, R. & Mahng, K. (2020). Numerical treatment of MHD flow. Computers, Materials & Continua. **66**(1), 229-245


https://doi.org/10.59568/JASIC-2023-4-1-02

[7] Eegunjobi, A. S. & Makinde, O. D. (2020). Thermodynamics Analysis of an MHD. Engineering Transactions. **68**(3), 239-252.

[8] Rao M. E. & Screnadh, S. (2017). MHD flow of a Casson fluid. Global Journal of pure and applied mathematics. **13**(10), 7529-7548.

[9] Hymavath, T. & Sridhar W. (2016). Numerical Solution on MHD. Int. J. Chem. Sci. **14**(4), 2183-2197.

[10] Chinyoka, T; Makinde, OD(2015). Unsteady and porous media flow. .*Inter. J. Numer.Methods for Heat and Fluid Flow*. 7 (1):1682-1704.

[11] Chinyoka, T; Makinde, OD (2012).Unsteady hydrodynamic flow. *Inter. J. Numer. Methods in Fluids*. 69:353-365.


https://doi.org/10.59568/JASIC-2023-4-1-02